ASTRONOMY & ASTROPHYSICS
SUPPLEMENT SERIES

Astron. Astrophys. Suppl. Ser. **139**, 231–244 (1999)

A UKST survey of blue objects towards the galactic centre – a search for early-type stars

P.L. Dufton[1,⋆], **S.J. Smartt**[2], **and N.C. Hambly**[3,4]

[1] The Department of Pure and Applied Physics, The Queen's University of Belfast, Belfast BT7 1NN, N. Ireland
[2] Isaac Newton Group of Telescopes, Apartado de Correos 368, E-38700, Santa Cruz de La Palma
[3] Royal Observatory, Blackford Hill, Edinburgh EH9 3HJ, Scotland, UK
[4] Institute for Astronomy, University of Edinburgh, Blackford Hill, Edinburgh EH9 3HJ, Scotland, UK

Received April 21; accepted June 30, 1999

Abstract. We have begun a search for early-type stars towards the galactic centre which are potentially young objects situated within the inner few kiloparsecs of the disk. U and V (or I) band photographic photometry from the UK Schmidt Telescope has been obtained to identify the bluest candidates in nineteen Schmidt fields (centred close to the galactic centre). We have spectroscopically observed these targets for three fields with the FLAIR multi-fibre system to determine their spectral types. In particular, ten early B-type stars have been identified and equivalent width measurements of their Balmer and He I lines have been used to estimate atmospheric parameters. These early-type objects have magnitudes in the range $11.5 \leq V \leq 16.0$, and our best estimates of their distance (given probable highly variable reddening in this direction together with errors in the plate photometry) suggest that some of them originated close to (i.e $R_g < 3$ kpc), or even beyond the galactic centre. Future high-resolution spectroscopy of these stars will provide reliable atmospheric parameters and element abundances, in order to map the current chemical composition of the inner galaxy.

Key words: stars: early-type — stars: fundamental parameters — stars: imaging — galaxy: center

1. Introduction and rationale behind the survey

Massive, early-type stars are central to investigations of the chemical composition and recent evolutionary history of galaxies (see, for example, the recent review by Kudritzki 1998). Their usefulness stems from their large luminosities and short lifetimes. The former allows even main sequence stars to be observed at high spectral resolution and signal-to-noise in distant regions of our galaxy (Dufton 1998), and in nearby galaxies such as the Magellanic System (Rolleston et al. 1993, 1996). Indeed early-type supergiants (with luminosities up to 10^6 that of the Sun) can now be observed in galaxies such as M 31 and M 33 (McCarthy et al. 1995; Monteverde et al. 1997), with lower resolution observations possible for even more distant galaxies, e.g. the preliminary results for NGC 2403 reported in Kudritzki (1998). Their short evolutionary lifetimes (typically 10 million years) then ensure that early-type stars provide information on the "current" status of the host galaxy.

B-type main-sequence stars, although fainter than O-types, have the additional advantage that their atmospheres can be modelled with sufficient reliability to yield accurate atmospheric parameters and chemical compositions (see, for example, Gies & Lambert 1992; Kilian 1992). Estimates are also less subject to the uncertainties implicit in other methods, such as dust affecting abundances from emission line plasmas (e.g. H II regions), or contamination from mixing with nuclear material processed from the stellar interior for highly evolved objects (e.g. Planetary Nebulae).

Our investigations of the chemical composition of the galactic disk have concentrated mainly on the anticentre direction, with evidence for small scale spatial structure (Smartt et al. 1996a, 1996b), the first reliable stellar estimate of large scale abundance gradients (Smartt & Rolleston 1997) and the use of element abundance ratios to identify the predominant nucleosynthetic environment, e.g. supernovae, low or high mass stars (Hibbins et al. 1998). By contrast, studies towards the galactic centre have been hampered by the large extinction at optical wavelengths. However, preliminary investigations of stars with galactic latitudes $2^\circ \leq |b| \leq 10^\circ$ have shown that it is possible to map both

Send offprint requests to: sjst@ing.iac.es
⋆ On leave of absence at the Isaac Newton Group of Telescopes, Apartado de Correos 368, E-38700, Santa Cruz de La Palma.

the inner region of the galaxy (Smartt et al. 1999) and even beyond the galactic centre (Ryans et al. 1997).

In these last two papers (and also in Venn et al. 1998), we have used the catalogues of southern luminous stars by Reed (1993) and Reed & Beatty (1995) to search for early-type candidates. Using a combination of colour-colour and colour-magnitude criteria, we identified a number of apparently normal B-type main-sequence stars within ∼4 kpc of the galactic centre (Smartt et al. 1999), together with A-type supergiants (their evolutionary descendents), which are slightly closer to the Sun. However this procedure was not straightforward as the catalogues have a faint visual magnitude cut-off of ∼12.5 and may not be complete. Additionally we now believe that we have exhausted the available published photometry for these galactic directions (at least for the colour and magnitude criteria appropriate for blue stars within the inner few kiloparsecs of the disk). Hence in order to further theses studies, we need to identify more potential targets which necessarily requires a (very) wide-field survey technique employing both multi-colour photometry and preliminary low-resolution spectroscopy for spectral-type classification.

The UK Schmidt telescope provides appropriate instrumentation to fulfill our needs. In this paper, we present the first results of a systematic survey to identify further early-type stars towards the galactic centre using its imaging and spectroscopic capabilities. Suitable photographic material for a mosaic of 19 Schmidt fields (yielding a total survey area of 475 square degrees) has already been obtained, and we have measured a subset of 14 of these fields, to produce lists of candidate blue stellar objects. For three fields, low dispersion multi-object spectroscopy of the blue targets has been gathered and we present the photometric and spectroscopic details associated with these three fields. It is intended that spectroscopy will be obtained for the other fields and these will be presented in future papers. The data reported here forms the basic selection criteria for a high resolution spectroscopic campaign to map the chemical composition of the inner galaxy.

2. Observational data

The observational data fall into two parts, viz. U and V (or I) band photographic plates or films and low dispersion multi-object FLAIR spectroscopy. Both datasets were obtained using the United Kingdom Schmidt Telescope at the Anglo-Australian Observatory (Siding Springs, New South Wales, Australia) and are discussed separately below.

2.1. Photographic photometry

Figure 1 shows the galactic centre survey region, and the fields (labelled with standard the UK Schmidt field numbers – see, for example, Tritton 1983) for which we have obtained photographic plate material. Field 456 (containing Baade's Window) was surveyed using existing U and I plate material; all other fields were surveyed using existing short exposure V plates taken for another project along with new U films obtained specially for this work. The new U-material was taken during the period April-August 1997 by staff at the UKST.

Table 1. The 19 Galactic Centre Survey fields

Field No.[1]	RA DEC (J2000.0)	Photographic film or plate numbers	SC[2]	Sp[3]
180	17 07 06 −55 09	U17516, V11803	n	n
226	16 33 48 −50 06	U17514, V12595	n	n
228	17 33 53 −50 02	U17565, V12124	y	n
275	15 55 31 −45 09	U17526, V11796	n	n
279	17 47 41 −45 01	U17597, V11811	y	n
331	16 31 26 −40 06	U17533, V11896	y	n
333	17 23 29 −40 03	U17527, V12099	y	n
391	16 51 18 −35 05	U17503, V12554	y	n
393	17 39 20 −35 02	U17534, V11839	y	b
454	17 18 12 −30 03	U17570, V12122	y	b
456	18 04 12 −30 00	U10278, I15587	y	b, r
520	17 39 05 −25 02	U17575, V12134	y	n
522	18 23 05 −24 58	U17571, V12058	y	n
589	17 53 58 −20 01	U17656, V11861	y	n
591	18 35 58 −19 57	U17605, V11963	y	n
661	18 02 52 −15 00	U17634, V12148	y	n
663	18 42 51 −15 00	U17576, V11296	y	n
807	18 42 40 −04 57	U17585, V11324	n	n
736	19 02 45 −09 56	U17598, V11297	n	n

[1] Standard United Kingdom Schmidt Telescope field numbers are defined in Tritton (1983); see also the UKSTU online catalogue at http://www.roe.ac.uk/
[2] Indicates if photographic material has been scanned on SuperCOSMOS, processed and blue objects selected.
[3] Indicates if spectra have been obtained, and if so, in which wavelength regions; b – 3860 − 4640 Å, r – 5400 − 6900 Å.

The pattern of fields in Fig. 1 resulted from maximising area coverage, at the same time minimising overlap (i.e. by choosing alternate fields) with the additional requirement that a short exposure V plate existed. In all, 19 fields make up this survey and Table 1 gives details of the photographic material.

The photographs were scanned using the precision microdensitometer SuperCOSMOS (see, for example, Hambly et al. 1998). To date, plate pairs for the 14 fields nearest the galactic centre have been measured (see Table 1). SuperCOSMOS digitises each plate at 10 μm (0.67″) resolution, 15–bit grey levels in ∼2.5 hours; offline software then processes the pixel map into a parameterised image list for all images detected above

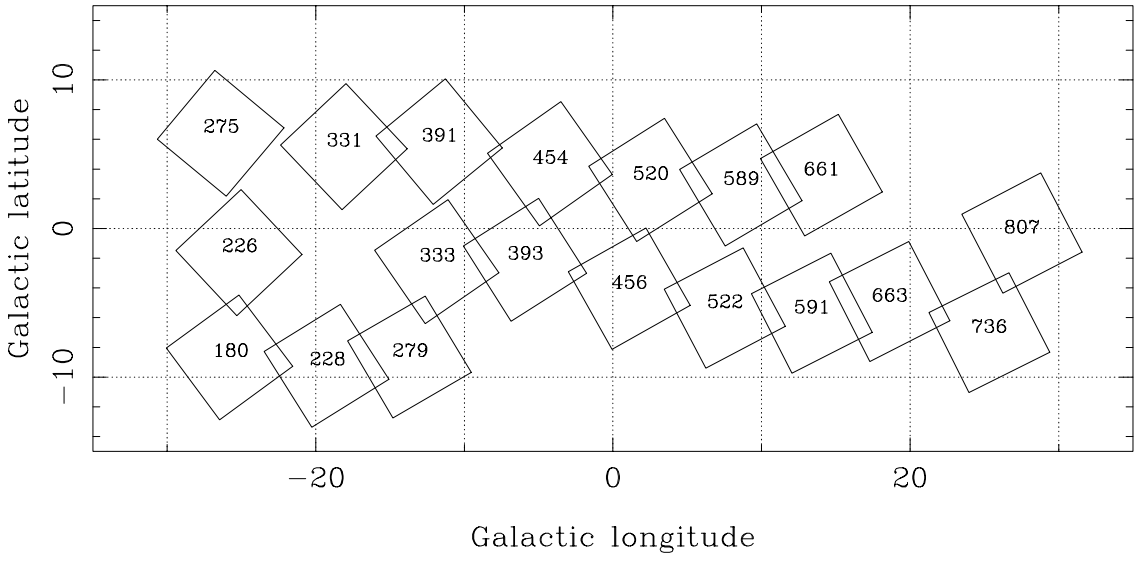

Fig. 1. The 19 Schmidt fields in the galactic centre survey. Galactic longitude is with respect to the galactic centre; field numbers are standard UKSTU field designations described in Tritton (1983)

a preset threshold. Every image has 32 parameters including celestial co-ordinates, shape and instrumental magnitude. Deblending software (Beard et al. 1990) rethresholds the pixel data during processing to detect and unscramble merged objects which is vital at these low galactic latitudes. Global astrometry over each field is achieved via Tycho–ACT catalogue standards (Urban et al. 1998). The accuracy of the resulting celestial co-ordinates is typically $0.25''$.

Plate pairs were reduced as follows. The individual image catalogues were paired using a search radius of $3''$. Poor quality images, parent images of deblends and elliptical images were all excluded from further analysis. An approximate calibration of the V–band instrumental magnitudes was obtained by fitting instrumental magnitudes versus V photometry from the Tycho stars in each field. In the case of field 456, an I–band photometric sequence was compiled using photometry presented in Blanco & Blanco (1984); Walker & Mack (1986) and Szymanski et al. (1996). No independent data were available for calibration of the U–band photographic instrumental magnitudes; hence in order to make the blue object selection in each field, we used the raw $u - v$ (or $u - i$ in the case of field 456) colour index as an indicator of spectral type. In general, the instrumental magnitudes measured from photographic plates are non–linear with respect to true apparent magnitudes due to difficulties in intensity calibration and the limited dynamic range during measurement. This results in raw instrumental colours ($u - v$, $u - i$) having, in general, zero–point offsets, which are functions of magnitude; in addition, photometric errors increase with object faintness. These in turn result in colour–magnitude diagrams in which the locus of the modal colour of the dominant F/G–type dwarfs is not vertical (i.e. not at constant colour) and in which the scatter about that locus increases with magnitude. Any selection of blue objects must take these into account, cf. the blue object selection procedure detailed by Stobie et al. (1997). Here, we adjusted the raw colours as a function of magnitude so that the locus of the modal stellar colour *minus* the width of the distribution (estimated on it's blue side) was at zero colour. This then allowed us to select the 80 bluest stars in each field in the range $11.5 < V < 16$ regardless of magnitude and in a consistent manner from field to field (the number of targets was chosen to be compatible with the FLAIR spectrograph - see Sect. 2.2). A typical pseudo colour–magnitude scatter plot is shown in Fig. 2 for field 393. However, note that these adjusted colour indices (also listed in Tables 2 to 5) are not true colours — they merely reflect relative colour between stars of similar magnitude.

The relative accuracy of these colours is estimated to be at best $\sim 0.2^{\rm m}$; however position–dependent systematics of several tenths of a magnitude or more are doubtless present. Moreover, crowding increases the scatter in the photometry, and there will inevitably be some cool stellar contamination in these selections. Such erroneously blue objects are of course weeded out via low–resolution spectroscopy, as discussed below. Note also that because the fields are very crowded and because the deblending algorithm is limited by the seeing on the plates (typically $\sim 2''$) many overlapping images will be discarded and completeness is likely to be significantly compromised — for example, Beard et al. (1990) estimate completeness of $\sim$70% at $|b| = 5°$. However, for our ultimate goal of identifying early–type stellar candidates in the region of the galactic centre for abundance studies, completeness is not a major consideration. Table 1 lists the UKST fields for which we have obtained U-material and indicates which fields have

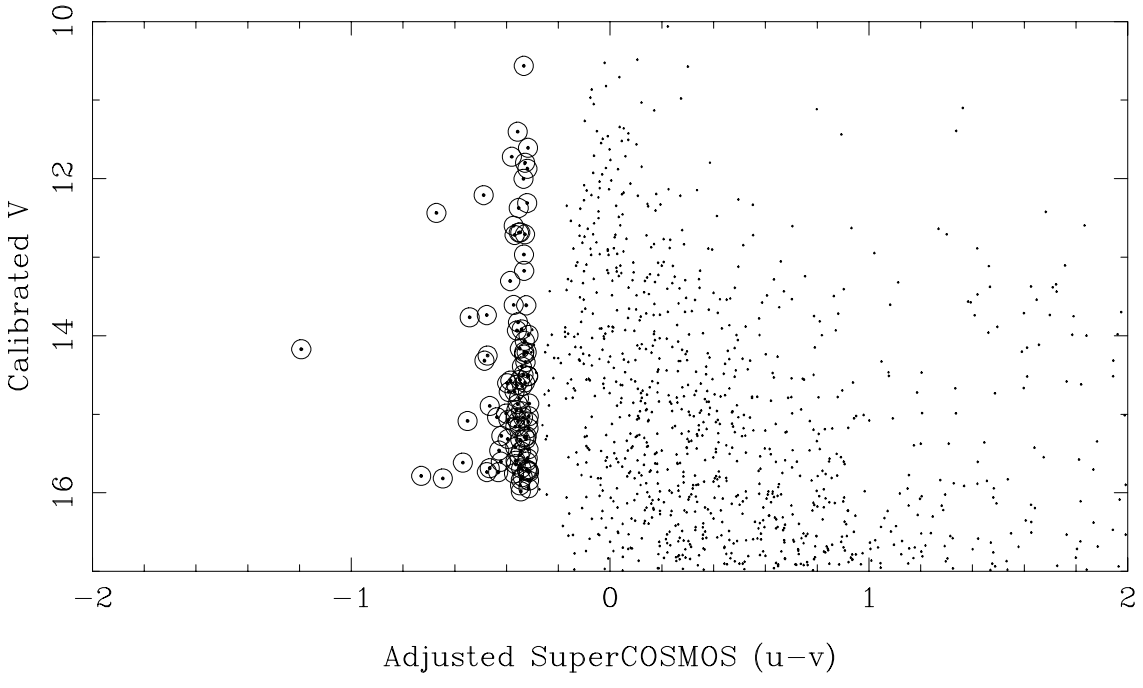

Fig. 2. A pseudo colour–magnitude scatter plot for field 393 (see text). The 100 bluest candidates are circled, while only 1000 other stars are plotted to illustrate the general scatter in this diagram

already been scanned. The photometric data are available from the authors on request for the 3 fields which are presented here.

2.2. Low resolution spectroscopy

For the blue candidates, identified from the photographic photometry, low resolution spectroscopy was undertaken using the FLAIR instrument on the UK Schmidt Telescope at Siding Springs. Eight nights were allocated in June 1997 but due to weather conditions observations were only possible on three nights; consequently only three of the 14 fields measured and processed with SuperCOSMOS were observed. The FLAIR system allows the simultaneous observation of up to 90 objects (from which target and sky fibres need to be allocated) with the 100 μm diameter fibres (or up to 150 objects using the 50 μm fibres) subject to limitations imposed by the finite size of the fibre ferrules and prisms. For the observations discussed here, the 100 μm fibre bundle was used and between 30 and 50 fibres were positioned on stellar targets with typically 10 sky positions. The prioritisation of targets was primarily based on their colours, with the very blue targets only being excluded if proximity to a bluer star made this necessary. Spectra, covering the wavelength region from approximately 3860 to 4640 Å, were obtained using the 1200B grating for all three fields at a spectral resolution (full-width-half-maximum) of approximately 2.7 Å. For Field 456, further red spectroscopy covering approximately 5400 to 6900 Å at a resolution of approximately 5.9 Å was obtained using the 600R grating. The FLAIR CCD is an EEV thinned and back-illuminated device, with 22 μ pixels in a 400×578 array (with the long axis along the spectral direction). Further details of the FLAIR instrument can be found in Parker & Watson (1994).

Stellar exposures were split into 1800 s segments, in order to reduce the impact of cosmic-ray events. Tracking of the Schmidt was typically good across approximately 4 hr either side of the meridian, but weather prevented the full exposure time being utilised. A total of 8×1800 s exposures were obtained for Fields 393, 454 and 456 in the blue region, plus for the last field 3×1200 s in the red. The seeing was generally poor, varying from $3''$ upwards on the three nights. The target exposures were bracketed with arc frames of Hg+Cd+Rb (for the blue region) and Hg+Cd+Ne (for the red region), and dome flat fields where taken for each setting (twilight flats, while preferable were not possible due to weather constraints). Preliminary data reduction was undertaken using the AAO's FLAIR package within the IRAF environment (Drinkwater & Holman 1996). As no structure was found in the bias frames, bias subtraction was achieved using the median integer bias value for the on-sky and the flat field frames. The target data frames were combined to remove cosmic-ray events using suitable clipping algorithms, in consecutive groups of 2-3 frames to ensure the signal levels in each were similar. The difference between frames combined with and without sigma-clipping showed the expected random patterns, indicating

that rejection of real signal had not occurred. An aperture identification file, created when the fibres where placed on each object, was used to assign slit positions to either an object or sky. The IRAF package `dofibers` (Valdes 1992) was used to extract the 1D spectra from each combined image, correct for the fibre-to-fibre variation in throughput (from the flat-field response frames), sky subtract, and then wavelength calibrate the final product. No traditional "flat-fielding" which removes the pixel-pixel CCD variations was performed, in line with normal fibre reduction procedures. Only five arc lines were visible in the blue region of the spectrum, but the pixel-wavelength relation is quite linear in the FLAIR spectrograph, and produced a RMS of 0.06 Å. In the red, the rich neon spectrum (∼26 lines) produced a RMS of 0.07 Å.

The spectra from the blue stellar candidates are summarised in Tables 2 to 5 for the three fields observed. In the first are listed co-ordinates, magnitudes and colours for those targets for which no fibres were placed (due to crowding or to a relatively low priority based on colour). The last three tables list for each field the corresponding information for stars which were observed spectroscopically. A complete library of the spectral data is available on request from the authors.

3. Analysis

3.1. Spectral types

The reduced spectra were input into the STARLINK package, DIPSO (Howarth et al. 1993) for further analysis. Initially the aim was to provide approximate spectral types for all the spectra which had a sufficient signal. Because of our interest in identifying early-type objects and given the relatively low spectral resolution and signal to noise ratio of our spectra, the following scheme was used to guide the classification.

O-type: Presence of He II lines at 4200 and 4541 Å (note that no stars of this type were identified).

Early-B-type: Relatively weak and narrow Balmer lines coupled with well developed neutral helium spectrum. The Ca II line (at 3933 Å), Mg II close doublet (at 4481 Å) and (if observed) the Na I doublet at 5890 Å should all be weak or absent (the interstellar components in the Ca II and Na I lines should normally appear weak at this spectral resolution).

Mid-B-type: Stronger and broader Balmer lines coupled with a weak but still distinct neutral helium spectrum. The Ca II, Mg II and Na I features, if present, are weak (with, for example, the He I line at 4471 Å being stronger than Mg II).

Late-B/A-type: Strong and broad Balmer lines coupled with either a very weak or absent neutral helium spectrum. Normally moderate Ca II, Mg II and weak Na I

Table 2. Blue stellar candidates for which spectroscopy was not obtained. For field 456, the magnitudes are in the I-band and colours are $(u-i)$ as explained in the text

Field	Star	RA (2000)	Dec	V	$(u-v)$
393	2	17 30 6.99	−33 41 40.5	15.80	−0.73
	4	17 44 57.97	−35 32 0.8	15.83	−0.65
	8	17 30 3.52	−33 45 1.8	12.23	−0.49
	16	17 43 13.16	−32 39 58.3	15.76	−0.43
	19	17 51 57.64	−34 47 0.3	15.29	−0.42
	26	17 43 3.98	−33 2 30.2	14.59	−0.39
	29	17 44 24.54	−33 10 19.6	13.63	−0.37
	30	17 42 30.68	−35 30 35.1	15.77	−0.37
	40	17 42 32.37	−32 52 11.1	13.95	−0.36
	42	17 43 40.44	−33 40 52.4	14.89	−0.36
	46	17 46 14.62	−34 24 21.7	12.70	−0.35
	47	17 43 15.76	−33 19 29.1	14.81	−0.35
	48	17 43 39.30	−33 1 2.3	15.54	−0.35
	51	17 43 15.27	−32 43 32.2	14.58	−0.35
	52	17 34 34.39	−37 0 6.6	15.92	−0.35
	57	17 44 1.36	−32 37 11.9	15.85	−0.35
	58	17 45 39.31	−34 40 25.1	14.98	−0.35
	59	17 30 52.08	−35 34 5.9	15.71	−0.35
	60	17 46 52.84	−36 32 8.5	13.94	−0.34
	61	17 37 15.81	−33 34 43.9	14.41	−0.34
	62	17 46 34.99	−34 22 27.3	14.66	−0.34
	63	17 49 33.42	−33 52 39.1	15.82	−0.34
	64	17 46 42.09	−34 7 19.5	15.06	−0.34
	65	17 47 6.07	−34 19 20.4	14.51	−0.34
	66	17 44 47.69	−35 10 19.5	12.02	−0.34
	67	17 29 52.01	−33 40 0.3	10.58	−0.34
	68	17 46 46.18	−33 19 31.2	12.98	−0.33
	69	17 33 11.12	−36 21 3.7	14.26	−0.33
	70	17 51 24.41	−35 1 18.0	13.19	−0.33
	71	17 48 2.80	−33 46 58.2	14.22	−0.33
	72	17 40 47.90	−32 32 43.0	15.31	−0.33
	73	17 45 1.53	−32 54 57.4	14.08	−0.33
	74	17 44 59.06	−35 4 3.3	12.73	−0.33
	75	17 36 12.28	−33 14 14.1	14.61	−0.33
	76	17 45 50.87	−33 29 16.3	11.81	−0.33
	77	17 43 29.36	−33 51 56.7	14.35	−0.33
	78	17 44 6.17	−32 58 23.9	15.33	−0.33
	79	17 43 41.72	−33 0 29.6	13.63	−0.33
	80	17 40 14.07	−32 51 57.0	15.30	−0.32
454	07	17 27 24.37	−29 21 14.0	15.85	−0.50
	19	17 26 43.47	−29 6 12.4	11.06	−0.37
	20	17 11 40.93	−30 28 49.3	14.87	−0.36
	21	17 26 19.28	−29 32 31.7	11.60	−0.36
	23	17 9 0.71	−28 34 50.1	13.57	−0.35
	31	17 25 10.00	−30 17 35.9	14.69	−0.34
	33	17 8 47.37	−30 25 39.4	14.24	−0.34
	35	17 16 41.20	−31 2 22.3	13.21	−0.34
	37	17 23 52.34	−30 33 59.1	12.06	−0.33
	40	17 9 19.10	−28 26 31.1	14.00	−0.33
	41	17 19 25.33	−30 53 59.8	11.65	−0.33
	42	17 25 34.50	−29 44 26.6	10.16	−0.33
	43	17 7 44.68	−29 18 15.3	15.94	−0.33
	44	17 25 10.96	−28 8 53.5	13.03	−0.33
	45	17 9 39.34	−28 55 11.6	15.43	−0.33
	46	17 24 35.89	−31 35 17.4	12.15	−0.33
	47	17 16 15.33	−31 40 32.3	10.93	−0.33

Table 2. continued

Field	Star	RA (2000)	Dec	V	$(u-v)$
454	48	17 24 14.29	−30 52 2.8	14.89	−0.33
	49	17 25 48.61	−28 14 42.4	12.01	−0.32
	51	17 16 24.66	−32 8 2.8	11.45	−0.31
	52	17 27 26.20	−30 5 57.1	14.50	−0.31
	53	17 9 23.90	−28 18 36.4	13.96	−0.31
	54	17 27 25.78	−29 56 31.9	14.90	−0.31
	55	17 27 6.28	−28 48 9.8	13.64	−0.31
	56	17 25 17.77	−30 37 6.4	15.86	−0.31
	57	17 8 41.32	−28 39 27.8	14.66	−0.30
	58	17 24 19.01	−31 56 53.2	15.30	−0.30
	59	17 27 29.31	−29 47 12.6	10.67	−0.30
	60	17 26 14.25	−28 19 18.0	15.10	−0.30
	61	17 29 53.34	−29 46 39.1	10.78	−0.30
	62	17 15 13.96	−31 34 20.0	11.74	−0.30
	63	17 28 58.07	−29 40 58.2	10.81	−0.30
	64	17 10 45.70	−28 39 36.5	15.93	−0.30
	65	17 29 2.44	−29 51 33.5	11.95	−0.29
	66	17 9 34.98	−28 18 24.9	13.32	−0.29
	67	17 25 25.21	−31 52 28.5	15.30	−0.29
	68	17 23 44.90	−31 41 44.9	15.09	−0.29
	69	17 15 11.96	−28 19 58.6	15.82	−0.29
	70	17 9 1.54	−28 27 58.2	14.14	−0.29
	71	17 8 58.43	−29 0 37.4	15.84	−0.29
	72	17 8 28.11	−28 34 18.9	12.73	−0.29
	73	17 25 23.75	−30 12 46.2	12.79	−0.29
	74	17 10 36.97	−28 53 6.9	14.76	−0.29
	75	17 9 21.56	−29 0 47.1	15.30	−0.29
	76	17 27 14.46	−30 14 1.4	14.87	−0.29
	77	17 7 35.47	−29 28 41.3	14.87	−0.29
	78	17 23 24.99	−30 10 4.5	12.08	−0.29
	79	17 26 20.06	−29 31 51.8	11.24	−0.29
	80	17 27 0.68	−28 47 30.8	10.01	−0.29
456	1	18 13 55.15	−29 5 5.8	15.03	−1.15
	14	18 15 6.90	−29 19 39.7	15.93	−0.69
	17	18 10 46.18	−30 43 7.0	15.16	−0.52
	24	18 4 23.08	−28 42 14.8	11.85	−0.17
	32	18 12 41.00	−30 30 47.6	14.97	0.00
	35	18 10 29.34	−30 54 18.9	15.86	0.03
	38	18 15 46.83	−30 45 9.6	13.48	0.10
	47	18 8 15.20	−32 28 23.9	15.19	0.22
	52	18 11 7.58	−31 44 21.1	14.99	0.26
	54	17 58 38.48	−28 48 18.6	12.86	0.30
	55	18 13 54.99	−29 15 47.0	15.83	0.30
	57	18 11 46.44	−31 33 27.4	15.96	0.31
	59	18 9 48.00	−32 1 3.7	12.86	0.33
	60	18 15 14.73	−29 2 21.9	15.39	0.35
	61	17 58 37.38	−28 46 18.5	15.10	0.36
	62	18 9 37.88	−30 56 2.2	15.97	0.36
	63	18 11 5.62	−28 5 17.0	12.86	0.37
	64	18 16 33.33	−29 34 46.6	15.51	0.37
	65	18 2 9.81	−30 29 8.5	12.57	0.38
	66	18 13 4.44	−28 10 15.8	15.82	0.39
	67	18 14 43.72	−28 30 17.9	12.76	0.41
	68	18 9 11.73	−32 12 27.0	15.05	0.42
	69	18 10 33.45	−30 30 7.6	12.65	0.42
	70	18 15 16.92	−30 55 47.3	15.76	0.42
	71	18 6 8.69	−28 59 5.0	12.93	0.43
	72	18 10 50.98	−31 28 12.4	15.82	0.43

Table 2. continued

Field	Star	RA (2000)	Dec	V	$(u-v)$
456	73	17 55 57.43	−30 51 28.0	15.89	0.44
	74	18 3 7.57	−28 51 33.5	12.98	0.44
	75	18 3 38.23	−28 47 53.9	15.67	0.44
	76	18 4 54.07	−28 41 23.4	12.70	0.44
	77	18 8 59.13	−31 9 6.1	14.39	0.44
	78	17 59 16.39	−28 58 40.0	13.18	0.46
	79	18 9 13.38	−31 50 7.8	12.52	0.46
	80	18 13 11.30	−28 36 34.0	14.76	0.46

features (with, for example, the Mg II doublet being at least as strong as the He I line at 4471 Å).

Late-type: Strong Ca II and Na I lines with the G-band present. No neutral helium lines visible.

Planetary Nebulae (PN): Balmer lines in emission with underlying continuum being weak. Often the neutral helium lines and the [N II] doublet at 6548 and 6583 Å are also observed in emission. We have cross identified any object showing strong emission lines with entries in the SIMBAD database, and some of them are already known PN. Note that at the available spectral resolution, the newly identified targets could also be post-asymptotic-giant-branch stars such as LSIV -12 111 (Conlon et al. 1993).

Subdwarf (sd): Strong Balmer lines coupled with the absence of Mg II or Ca II lines expected in late-B/A-type stars.

These criteria were only used as guides as sometimes features were not identifiable (possibly due to a low signal-to-noise ratio) and in a few cases the spectrum characteristics were inconsistent. Additionally our classification as "late-type", effectively covers all stars later than A-type. As our primary intention was to identify early-type stars, we have not attempted to further refine this classification.

The preliminary classifications are summarised for the three fields in Tables 3 to 5. Also listed are the mean stellar counts and a brief description of the spectrum. The counts refer to the wavelength ranges 3900 to 4600 Å in the blue and 5600 to 6800 Å in the red; the instrumental response is such that the extreme blue (3860 − 4000 Å) and red (6700−6900 Å) regions of the spectra had counts typically a factor of two less than these mean values. The gain of the CCD used in FLAIR is approximately 1 e^-/adu, hence the tabulated values are close to the number of detected photons; the signal-to-noise ratio of the stellar continuum can thus be estimated directly from them. Although there is a correlation between the mean counts and the photographic V (or I) magnitude, there are some significant discrepancies. These may in part be due to errors in the latter but we believe are mainly due to a combination of three factors. The first is the positioning of the fibres on the plate itself – although the fibres have a ∼7″ diameter on the sky, the semi-manual positioning method incurs placement inaccuracies. Secondly fibre to fibre through-put variation

Table 3. Preliminary identifications of targets in Field 393. For the two possible PN's identified in this field, no object in the SIMBAD catalogue was found within 2′ of their positions

No.	RA (2000)	Dec (2000)	V	$u-v$	Mean	Comment	Sp. Type
1	17 36 59.60	−36 56 40.6	14.19	−1.19	500	Moderate H I, no He I, no Mg II, no Ca II	sd?
3	17 49 59.91	−35 32 40.9	12.45	−0.67	200	Poor spectrum, weak H I, He I	early-B
5	17 48 8.61	−34 4 0.6	15.63	−0.57	40	No significant signal	-
6	17 39 35.70	−33 39 13.4	15.10	−0.55	220	Narrow H I, strong Ca II	late
7	17 49 2.49	−34 32 54.6	13.78	−0.54	140	Featureless spectrum	-
9	17 42 23.01	−35 47 56.8	14.34	−0.49	320	Narrow H I, strong Ca II, G-band	late
10	17 49 5.04	−34 52 52.1	13.75	−0.48	160	Narrow H I, strong Ca II, G-band	late
11	17 49 28.15	−35 59 52.7	15.75	−0.48	30	No significant signal	-
12	17 50 38.38	−34 40 45.5	14.27	−0.48	150	Poor spectrum, H I?, Ca II?, G-band?	late?
13	17 39 28.91	−33 32 46.2	15.70	−0.47	450	Weak H I, He I	early-B
14	17 51 8.23	−34 8 43.7	14.91	−0.47	40	No significant signal	-
15	17 32 57.44	−36 15 14.7	15.05	−0.44	250	Narrow H I, strong Ca II, G-band	late
17	17 48 16.78	−35 38 17.4	15.48	−0.43	60	H I emission, no other features	PN
18	17 37 9.21	−37 0 44.0	15.62	−0.42	10	No significant signal	-
20	17 42 37.86	−32 43 20.3	15.01	−0.40	70	Poor spectrum, weak H I?	-
21	17 44 20.18	−33 10 46.3	14.62	−0.40	60	Poor spectrum, weak H I?	-
22	17 41 51.01	−33 32 13.8	15.33	−0.40	90	Poor spectrum, G band?, Ca II?	late?
23	17 31 49.63	−36 32 10.7	15.09	−0.39	300	Narrow H I, strong Ca II, G-band	late
24	17 40 39.78	−35 6 53.7	14.73	−0.39	290	Strong H I, weak He I, Mg II?, Ca II?	mid/late-B
25	17 45 45.80	−33 25 47.8	13.32	−0.39	300	Strong H I, weak He I, Mg II?, Ca II?	mid/late-B
27	17 32 32.34	−32 56 37.5	11.74	−0.38	4500	Strong H I, weak He I, Mg II∼He I, Ca II	late-B
28	17 32 4.30	−33 9 20.6	12.62	−0.37	1500	Strong H I, no He I, weak Mg II, weak Ca II	sd?
31	17 43 27.30	−33 14 15.0	14.73	−0.37	30	No significant signal	-
32	17 48 58.41	−35 18 35.0	12.73	−0.37	480	Narrow H I, He I, Mg II?	early-B
33	17 40 54.35	−34 5 7.3	15.44	−0.37	60	Poor spectrum, Ca II?	late?
34	17 45 43.64	−32 53 33.1	15.18	−0.37	160	Narrow H I, strong Ca II, G-band	late
35	17 44 24.82	−32 44 44.5	15.61	−0.37	20	No significant signal	
36	17 32 39.05	−35 49 40.2	15.06	−0.37	180	Narrow H I, no He I, Ca II?, low g	late-B/A
37	17 44 54.80	−34 35 38.3	15.65	−0.37	100	Narrow H I, strong Ca II, G-band	late
38	17 43 42.53	−35 7 57.9	14.64	−0.36	160	Narrow H I, strong Ca II, G-band	late
39	17 31 24.88	−35 41 7.0	14.97	−0.36	110	Poor spectrum, weak H I	-
41	17 31 30.97	−33 14 49.9	11.42	−0.36	2400	Strong H I, weak He I, Mg II	mid-B
43	17 47 34.10	−33 31 16.9	15.11	−0.36	110	Poor spectrum, narrow H I, strong Ca II	late
44	17 41 19.61	−33 36 43.1	13.85	−0.36	130	Poor spectrum, narrow H I, strong Ca II	late
45	17 34 26.36	−33 3 33.4	12.39	−0.36	1600	Strong H I, He I?, strong Si II, Ca II	ABp
49	17 46 54.84	−33 47 48.2	15.17	−0.35	60	Poor spectrum, Ca II?, G-band?	late
50	17 48 49.28	−34 4 44.3	14.18	−0.35	120	Featureless spectrum	-
53	17 32 54.10	−33 48 59.5	12.70	−0.35	1500	Strong H I, He I, weak Mg II	mid-B
54	17 40 28.52	−34 5 18.9	15.35	−0.35	135	Featureless spectrum	-
55	17 32 21.89	−36 55 33.0	16.00	−0.35	170	Poor spectrum, narrow H I, He I?	early-B
56	17 34 42.09	−33 3 56.8	15.49	−0.35	200	H I emission, Ca II	PN?
58	17 45 39.31	−34 40 25.1	14.98	−0.35	100	Narrow H I, strong Ca II, G-band	late
59	17 30 52.08	−35 34 5.9	15.71	−0.35	180	Narrow H I, strong Ca II, G-band	late
60	17 46 52.84	−36 32 8.5	13.94	−0.34	40	No significant signal	-
61	17 37 15.81	−33 34 43.9	14.41	−0.34	330	Narrow H I, strong Ca II, G-band	late
62	17 46 34.99	−34 22 27.3	14.66	−0.34	180	Poor spectrum, weak H I, Ca II?, G-band	late
63	17 49 33.42	−33 52 39.1	15.82	−0.34	10	No significant signal	-
64	17 46 42.09	−34 7 19.5	15.06	−0.34	70	No significant signal	-

contributes significantly, and thirdly as field acquisition and rotation are achieved with five fiducial fibres fed to a direct viewing TV system, the positioning of the whole plate on the sky may cause differential discrepancies across the field.

The spectral descriptions are necessarily brief with the designation of lines as "strong", "weak" etc. being in the context of the whole dataset. In the case of field 456, the comments include both the red and blue spectra. The absence of lines may in some cases be due to the poor signal-to-noise ratio in the spectra; however an attempt was made to only search for lines that should have been visible. In Fig. 3, the range of quality of the spectra is illustrated for the field F456 (for which there are both blue and

Table 4. Preliminary identifications of targets in Field 454

No.	RA (2000)	Dec (2000)	V	$u-v$	Mean	Comment	Sp. Type
1	17 27 1.24	−29 21 31.7	15.41	−1.20	0	No significant signal	-
2	17 12 58.19	−29 53 20.2	15.38	−1.06	40	No significant signal	-
3	17 25 24.15	−30 35 24.1	15.52	−0.93	40	No significant signal	-
4	17 9 25.40	−28 32 20.2	15.26	−0.89	95	Narrow H I, no He I, Ca II, *G*-band	late
5	17 12 32.69	−28 44 33.5	15.94	−0.68	30	No significant signal	-
6	17 17 27.06	−30 22 14.4	15.73	−0.50	10	No significant signal	-
8	17 7 21.97	−30 12 21.2	14.60	−0.50	20	No significant signal	-
9	17 8 15.19	−29 18 38.6	15.31	−0.49	10	No significant signal	-
10	17 17 38.60	−28 40 56.7	12.21	−0.43	690	Narrow H I, He I, no Mg II, O II?	early-B
11	17 28 21.62	−29 34 56.1	12.03	−0.42	2300	Strong H I, He I?, Mg II	late-B
12	17 23 23.00	−31 16 29.8	14.48	−0.40	180	Poor spectrum, narrow H I, no He I, strong Ca II	late
13	17 27 8.01	−30 36 28.8	11.31	−0.40	4100	Moderate H I, moderate He I (HD 317573)	mid-B
14	17 21 5.64	−27 57 26.7	10.66	−0.39	4500	Moderate H I, moderate He I (SAO 185293)	mid-B
15	17 28 49.11	−28 56 49.6	15.32	−0.39	60	Poor spectrum, narrow H I, no other lines	-
16	17 18 32.50	−30 57 49.2	11.26	−0.39	3000	Strong H I, weak He I, Mg II∼He I, weak Ca II	late-B
17	17 25 39.68	−30 43 50.0	11.49	−0.39	3300	Strong H I, weak He I, Mg II∼He I, weak Ca II	late-B
18	17 20 40.89	−27 57 30.2	15.29	−0.39	20	No significant signal	-
22	17 9 27.94	−28 27 6.4	13.69	−0.35	40	Poor spectrum, narrow H I, no other lines	-
24	17 24 12.13	−31 45 4.7	10.52	−0.35	7500	Strong H I, weak He I, Mg II∼He (HD 317535)	late-B
25	17 10 14.70	−31 49 57.8	14.68	−0.35	40	No significant signal	-
26	17 8 49.05	−28 42 29.2	15.35	−0.34	10	No significant signal	-
27	17 14 25.59	−31 12 16.6	13.77	−0.34	160	Poor spectrum, narrow H I, marginal He I	early-B?
28	17 27 15.69	−29 48 32.6	14.74	−0.34	250	Narrow H I, no He I, Mg II?, Ca II, *G*-band	late
29	17 23 53.89	−30 19 25.9	15.58	−0.34	180	Strong H I, no He I, Mg II?, moderate Ca II	A
30	17 10 50.61	−28 40 16.5	15.85	−0.34	10	No significant signal	-
32	17 26 8.80	−30 8 12.8	11.70	−0.34	0	No significant signal	-
34	17 8 57.48	−28 53 44.5	13.42	−0.34	70	Poor spectrum, narrow H I, Ca II	late
36	17 18 59.81	−32 17 27.9	10.67	−0.33	1800	Moderate H I, moderate He I (CD−32 12597)	mid-B
38	17 19 1.44	−29 49 14.3	10.99	−0.33	2300	Strong H I, weak He I, Mg II∼He I	late-B
39	17 6 57.00	−29 21 37.6	15.25	−0.33	60	No significant signal	-
50	17 27 56.06	−31 4 9.1	11.19	−0.32	780	Strong H I, no He I, Mg II?, Ca II?	A, sd

red spectra); star 5 represents the lower range of usable spectra and star 58 the upper range. In the comments, the following abbreviations have been used, low g: gravity appears to be less than that of a main sequence star and the target may be either a giant/supergiant or an evolved object; He+: target may have an enhanced helium spectrum. In the comments, a question mark indicates that the line identification is marginal and possibly suspect, whilst for a spectral type, it implies that either the quality of the spectra or inconsistencies between different criteria puts the classification in significant doubt.

In Field 456, four of the blue objects showed PN type features with H I strongly in emission often accompanied with He I and S II emission lines. These were cross-identified with objects in the SIMBAD catalogue and all of them are previously known planetary nebulae (the PK designations are from Perek & Kohoutek 1967). The two objects in Field 393 which also show PN features do not have known counterparts, and hence are new identifications. We have also searched for known objects within a 20″ radius around the positions of all stars which have a V (or I, in the case of Field 456) magnitude brighter than 13. Four of the brighter stars in Field 454 were found to be known objects, while the rest of the stars in the sample have no other identifications, within the SIMBAD database. Star number 26 in Field 456 is LS4784 for which we already have high-resolution spectra (Smartt et al. 1999) and which appears to be a normal, distant, B-type star. Hence we included this star to test whether our methods would retrieve such an object. No attempt was made to cross-identify the rest of the sample with magnitudes below this cut-off. As these objects are generally unremarkable apart from being blue, they are unlikely to appear in any other catalogue.

For some of the stellar spectra, more detailed descriptions are appropriate and these are provided below:

Field 393, star 36: The Balmer lines are narrow and relatively weak and are compatible with an early-B-type classification. However, although the signal-to-noise ratio is relatively low, the absence of a neutral helium spectrum implies a later spectral type. The Ca II at 3933 Å appears to be present but its strength cannot be estimated. Hence this star is either a late-B/A-type with a low gravity or, less likely given the absence of the *G*-band, a late-type object.

Table 5. Preliminary identifications of targets in Field 456

No.	RA (2000)	Dec (2000)	I	$u-i$	Mean Blue/Red	Comment	Sp. Type
2	18 13 55.15	−29 5 5.8	15.03	−1.15	120/580	Weak H I, no He I, Ca II, Na I, *G*-band	late
3	18 9 53.65	−30 59 5.9	13.70	−1.12	210/330	Weak H I, strong He I, strong Na I	He+
4	18 11 5.03	−28 58 59.4	12.28	−1.10	70/300	Strong H I, He I, [S II] emission (PK002−042)	PN
5	18 13 57.40	−31 11 40.4	15.37	−1.10	100/100	Poor spectra, narrow H I, He I	early-B
6	18 7 53.89	−29 44 34.3	15.07	−1.09	80/430	Strong H I, He I, [S II] emission (PK001−042)	PN
7	18 12 30.36	−30 31 25.4	15.52	−1.05	120/150	Narrow H I, no He I, Ca II, Na I, *G*-band?	late
8	17 54 26.39	−28 34 7.4	14.16	−0.96	50/310	Poor blue spectra, broad H I, Na I	late?
9	18 2 26.17	−30 23 36.6	15.46	−0.93	120/590	H I, no He I, Ca II, Na I, *G*-band	late
10	17 54 51.88	−28 24 26.1	14.57	−0.92	30/200	Poor blue spectra, strong Na I	late?
11	18 10 7.74	−31 20 8.3	15.41	−0.92	50/50	Poor spectra, *G*-band?, Na I, H alpha	late?
12	18 8 59.87	−29 50 30.0	15.73	−0.85	80/700	Poor blue spectra, strong Na I, weak H alpha	late
13	18 15 6.58	−30 15 33.1	13.82	−0.80	90/290	Strong H I, He I, [S II] emission (PK002−062)	PN
15	18 13 19.96	−29 25 4.6	15.96	−0.67	90/340	Weak H I, no He I, *G*-band?, Na I	late
16	18 0 59.25	−28 45 49.8	11.55	−0.62	1200/2400	Strong H I, He I, Mg II∼He I, Ca II, Na I	late-B
18	18 10 33.60	−30 30 20.5	15.33	−0.40	120/150	Poor spectra, weak H I, He I?	early-B
19	17 59 54.24	−29 8 21.7	15.01	−0.34	140/860	Poor blue spectra, Ca II?, Hα emission, Na I	late
20	18 13 31.98	−28 38 2.4	15.31	−0.34	120/350	Very weak H I, Ca II, *G*-band?, strong Na I	late
21	18 7 7.30	−29 42 13.8	14.03	−0.27	260/480	No H I, no He I, no Ca II, Na I	late?
22	17 59 22.67	−28 43 53.1	12.14	−0.23	1100/2100	Strong H I, no He I, weak Ca II, Na I	A
23	18 4 23.08	−28 42 14.8	11.85	−0.17	1800/2100	Strong H I, He I, Mg II∼He I, weak Ca II	late-B
25	18 12 53.29	−28 34 7.8	14.49	−0.13	260/390	Weak H I & He I, C II?, Ca II, Hα em., low g	late-B
26	18 13 58.73	−30 29 31.6	11.97	−0.11	2100/440	LS4784	B2 IV
27	18 11 35.07	−28 22 37.3	12.87	−0.10	170/460	Strong H I, [S II] emission (PK003−047)	PN
28	18 8 40.16	−31 30 0.9	15.83	−0.09	180/540	Narrow H I, no He I, Ca II, strong Na I	A?
29	18 9 55.28	−29 21 55.3	14.74	−0.06	2800/920	Strong H I, Ca II, Na I	A
30	18 13 44.97	−30 58 31.1	15.95	−0.04	110/820	Poor blue spectra, weak H I, He I?	early-B?
31	18 4 16.88	−31 37 11.9	15.50	−0.03	90/320	Poor spectra, weak H I, no He I, Ca II, Na I	late?
33	18 12 41.06	−30 10 16.9	15.93	0.00	140/200	Poor spectra, moderate H I, He I?	mid-B
34	18 12 4.92	−31 10 36.7	15.70	0.02	140/410	Moderate H I, strong Ca II, Na I	late
36	18 15 14.38	−28 34 10.4	13.90	0.05	320/310	Moderate H I, He I?, Mg II?, Ca II, Na I	late-B/A
37	18 7 59.68	−28 33 23.7	12.24	0.09	820/1000	Strong H I, Mg II∼He I, Ca II?, Na I	late-B
39	18 5 27.05	−28 18 3.7	12.46	0.12	450/2500	Weak H I, He I, Ca II, Na I, He+?	early-B?
40	17 58 37.79	−28 44 26.1	14.44	0.13	190/860	Weak H I, H alpha emission, no He I, Na I	late?
41	18 0 46.50	−31 45 55.5	16.00	0.15	90/430	Poor blue spectra, weak H I, no He I, Na I	late?
42	18 4 43.23	−28 51 11.9	15.81	0.16	220/770	Weak H I, no He I, no Ca II, *G*-band?, Na I	late?
43	18 9 23.58	−31 21 6.9	12.66	0.17	1700/1300	Strong H I, He I, Mg II∼He I, weak Na I	late-B
44	18 16 31.16	−29 19 3.0	15.36	0.17	130/130	Poor spectra, weak H I, no He I, weak Na I	-
45	18 3 47.02	−28 52 32.8	12.48	0.21	1200/1900	Strong H I, He I?, Mg II>He I, Na I	late-B
46	18 0 28.89	−28 44 7.6	14.04	0.22	290 1300	Weak H I, no He I, Ca II, *G*-band, Na I	late
48	18 12 33.40	−28 51 3.6	14.48	0.22	80/270	Poor blue spectra, H alpha, Na I	late?
49	17 53 38.31	−30 20 29.1	15.97	0.23	80/390	Poor blue spectra, weak H I, *G*-band?, Na I	late?
50	18 8 6.90	−31 5 45.9	15.88	0.26	160/450	Weak H I, no He I, Ca II, *G*-band?, Na I	late
51	18 10 21.47	−29 6 1.9	12.50	0.26	930/520	Strong H I, He I?, Ca II, Mg II, Na I	late-B/A
53	17 55 50.03	−31 57 17.6	12.34	0.29	2900/1600	Strong H I, Mg II>He I, Ca II, Na I	late-B
56	18 6 2.06	−30 17 34.2	12.73	0.31	1900/3700	Strong H I, no He I/Mg II, weak Ca II/Na I	sd
58	18 2 34.72	−28 21 52.9	12.49	0.32	1300/2400	Strong H I, He I?, weak Ca II, Mg II, Na I	late-B/A

Field 393, star 45: The strong Balmer lines coupled with a marginal identification of neutral helium lines implies a late-B-type classification. However the Si II doublet near 4130 Å is very strong with Si II lines at 3954 Å and 4200 Å also present. Numerous other metal lines (including Mg II and Ca II) are present in the spectrum and we therefore classify it as Bp or Ap-type.

3.2. Early-type candidates

For the early-type candidates (designated at early-B, mid-B or late-B/A in Tables 3 to 5), an attempt has been made to obtain a more reliable classification and to estimate atmospheric parameters. Equivalent widths were estimated for the Balmer, Hϵ, Hδ, Hγ, lines by arbitrarily assigning the continuum level at ±16 Å from the line centre. Line strengths were also estimated for the neutral helium

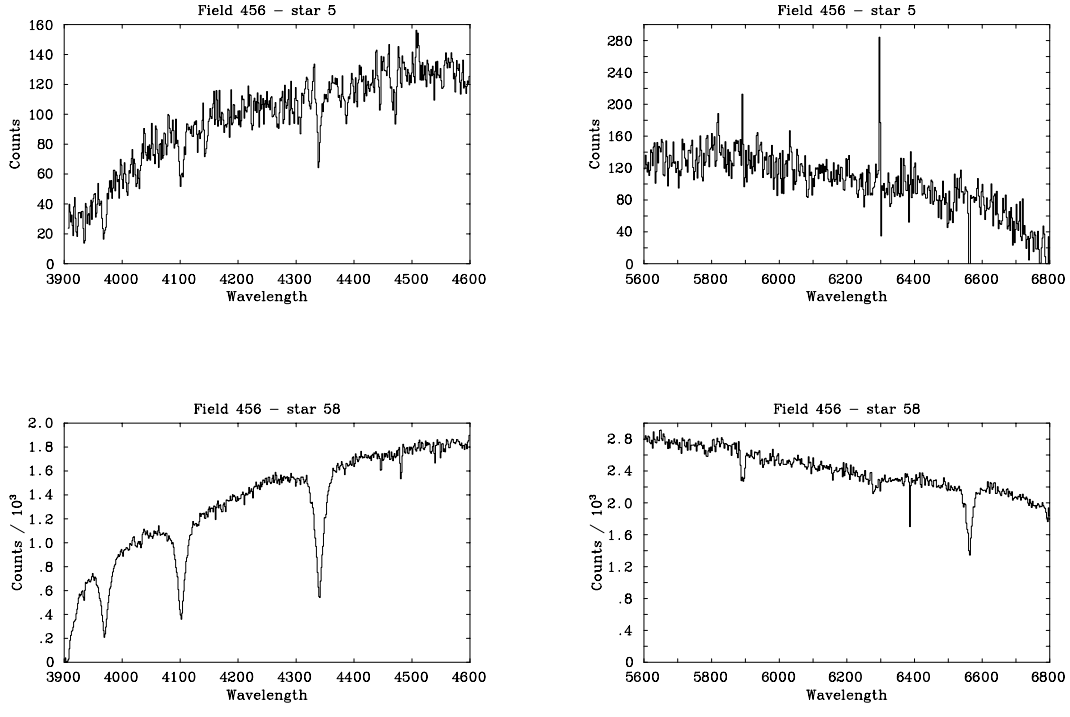

Fig. 3. Typical spectra are shown for two stars in the Field 456. Star 5 represents the lower range of usable data and has a signal to noise ratio of approximately 10, whilst star 58 is amongst the best spectra obtained with a signal to noise ratio of approximately 60

lines at 4026, 4143, 4387 and 4471 Å (with the continuum defined at ±8 Å) and metal lines, including Mg II at 4481 Å and Ca II at 3933 Å (with the continuum at ±4 Å). The equivalent widths are listed in Table 6, with ":" implying a marginal measurement, "p" that a line is present but its strength cannot be reliably estimated and "p?" that a line may be present. Where no estimate is provided, the line could not be identified *at the signal-to-noise and resolution of the spectrum.*

Assuming a normal helium to hydrogen ratio, the relative strength of the neutral helium and hydrogen lines can provide an estimate of the stellar effective temperature. We have used a grid of models generated with the ATLAS9 code of Kurucz (1991) and an LTE model atmosphere code to predict line strengths for these feature; further details of the methods can be found in, for example, Smartt et al. (1996b). The range of effective temperatures considered was from 10 000 to 30 000 K with logarithmic gravities from 4.5 dex down to near the Eddington limit and a helium to hydrogen fraction of 0.092 by number was assumed. When calculating equivalent widths, the continuum was defined so as to be consistent with the observational measurements.

Over this range of atmospheric parameters, the theoretical predictions for the equivalent width of the Balmer, Hδ and Hγ, lines normally agree to better than 5% (we did not consider Hϵ as it is blended and is in a spectral region, where the counts were normally low). Given the uncertainties in the observational data, we have therefore used just the mean in the equivalent width of the two lines (designated W_λ(H)) in our comparisons. We have also assumed that this would also be appropriate to the equivalent width of either line (when for example the measurement of the equivalent width of the other line was not possible).

The ratio of the strength of the neutral helium lines to W_λ(H) as a function of effective temperature is illustrated in Fig. 5, for the He I line at 4026 Å. Two logarithmic gravities, 3.0 and 4.0 dex, were considered; ratios are only available up to an effective temperature of 25 000 K for the former, due to the effect of radiation pressure. This ratio does not depend significantly on the adopted gravity. For example in the lower temperature regime a change of the gravity by 1.0 dex would affect the temperature estimate by normally less than 1000 K, while at higher temperatures, the ratio becomes temperature insensitive but again the limit does not significantly depend on gravity.

The behaviour of the ratios for the other observed helium lines is qualitatively similar and hence they can be used independently to estimate (or, at least, set a lower limit on) the effective temperature. Then the mean hydrogen line strength, W_λ(H), can be used to estimate the gravity. This procedure was employed for the targets listed in Table 6. However it became apparent that whilst the He I lines at 4026, 4143, 4387 Å gave consistent results (within the observational uncertainties), that at 4471 Å

Table 6. Equivalent widths for early-type candidates in fields 393, 454 and 456. Also listed are the estimated atmospheric parameters

Field	Star	Mean	3970	4101	4340	4026	4143	4387	4471	4481	3933	$T_{\rm eff}$	log g
Early B-type													
393	3	200	3.6:	3.6:	2.5:	1.3:	1.5:	1.0:	1.0:	-	-	$\geq$ 20 000	$\geq$ 3.2
393	13	450	4.5	3.8	3.5	1.5:	0.8:	0.8:	0.9:	-	-	$\geq$ 20 000	$\geq$ 3.4
393	32	480	6.0	4.5	4.0	1.3:	1.0	1.0	1.2	0.2:	0.5:	$\geq$ 20 000	$\geq$ 3.7
393	55	170	4.9	4.6	4.2	-	-	-	1.6	-	-	$\geq$ 20 000:	$\geq$ 3.8:
454	10	690	4.2	4.0:	3.7	1.1	0.7	0.8	1.1	-	0.5	$\geq$ 20 000	$\geq$ 3.5
454	27	160	5.3:	3.4:	4.0	0.9:	-	p	1.4:	-	-	$\geq$ 20 000:	$\geq$ 3.5:
456	5	100	6.4:	4.1:	3.8:	1.5:	p	1.0:	1.6:	p?	p?	$\geq$ 20 000:	$\geq$ 3.5
456	18	120	6.7:	5.6:	4.4:	-	0.6:	0.8:	0.9:	0.3:	-	18 000:	4.0:
456	30	110	8.8:	5.3:	4.4:	-	-	0.9:	-	-	p?	18 000:	4.0:
456	39	450	3.8	3.4	3.1	0.8:	p	0.7	1.2	p	0.7:	$\geq$ 20 000	$\geq$ 3.3
Mid B-type													
393	24	290	-	p	5.0	p	p	-	-	p?	-	$\leq$ 15 000	$\leq$ 3.5:
393	25	300	8.7	6.9	6.7	0.5:	p?	0.3:	0.3:	p?	-	12 000	3.6
393	27	4500	7.7	7.3	7.4	0.5:	p?	0.2:	0.3:	0.3:	0.3:	11 000	3.4
393	41	2400	6.9	5.2	5.3	-	p?	0.3:	0.5:	0.2:	0.2:	12 000	3.0
393	45	1600	9.6	9.1	9.0	p?	0.4:	-	0.5:	0.4:	1.1	12 000	4.0
393	53	1500	7.7	7.0	6.9	0.9	0.4:	0.5:	0.8	0.3	0.4:	14 000	4.3
454	13	690	6.7	6.3	5.9	1.0	0.5:	0.6	0.9	0.2	0.3:	15 000	4.0
454	14	4500	5.3	5.2	4.8	0.9	0.4:	0.6	0.9	0.2	0.2	15 000	3.5
454	16	3000	6.9	6.8	6.8	0.3:	p	0.2	0.2	0.2	0.2	11 000	3.2
454	17	3300	7.6	7.5	7.2	0.3	p	0.2	0.3	0.2	0.3	11 000	3.4
454	24	7500	7.4	7.3	7.0	0.2	0.1:	-	0.3	0.2	0.3	11 000	3.3
454	36	1800	7.3	6.7	6.5	0.9	0.4	0.4	0.8	0.2	0.2	14 000	4.0
454	38	2300	7.9	7.5	7.4	0.3:	0.3	0.2	0.5	0.3	0.3	12 000	3.8
456	16	1200	6.5	6.4	6.1	0.4:	p	0.3:	0.3:	0.2	0.3	12 000	3.3
456	25	260	5.9	5.0	4.9	p	-	0.5:	0.5:	-	0.8:	15 000	3.5
456	33	140	8.4	6.7	6.0	1.1:	0.4:	-	0.4:	0.4:	-	15 000	4.2
456	37	820	7.2	6.1	5.7	0.7:	0.5:	0.7:	0.6:	0.3:	0.2:	16 000	4.1
456	43	1700	7.6	7.8	6.8	0.2:	-	0.2:	0.3:	0.2:	0.3:	11 000	3.4
456	53	2900	7.0	6.9	6.8	0.3	-	p?	0.3:	0.2:	0.2:	11 000	3.1
Late B or A-type													
393	1	500	3.9	4.4	4.3	-	-	-	-	-	-	$\leq$ 13 000	$\leq$ 2.7
393	28	1600	9.9	8.5	8.5	-	-	-	-	0.3:	0.7	$\leq$ 12 000	$\leq$ 4.3
454	11	2300	9.4	8.8	8.4	-	-	-	-	0.3	0.2	$\leq$ 12 000	$\leq$ 4.3
456	36	320	6.1:	6.0	5.0	-	-	p?	-	0.5:	0.8:	$\leq$ 13 000	$\leq$ 3.2
456	45	1200	10.3	8.6	8.1	p?	-	-	0.2:	0.3	1.0	$\leq$ 12 000	$\leq$ 4.2
456	51	930	10.3	9.5	8.6	-	-	0.2:	0.2:	0.4	0.7	$\leq$ 12 000	$\leq$ 4.5
454	58	1300	9.6	8.9	8.7	p?	p?	p?	-	0.4	0.4	$\leq$ 12 000	$\leq$ 4.4

Endflushleft: Command not found.

led to consistently lower temperatures estimates (by typically 2000 K). This discrepancy probably reflects a systematic over estimate in the theoretical equivalent widths for this line; hence we gave this ratio lower weight when finalising our atmospheric parameters estimates, which are summarised in Table 6.

We note that, even for the best observed stars, there will be considerable uncertainties in the atmospheric parameters. Realistic errors estimates would be at least $\pm 1000 - 2000$ K in effective temperature and $\pm 0.2 - 0.3$ in the logarithmic gravity. The uncertainties for the lower quality spectra could be larger. However, this is still sufficient for us to classify a star and, in particular, decide whether it is suitable for further high resolution spectroscopy. Figure 4 shows the blue spectra of the stars that we have identified as early-types in Table 6. Also shown for comparison purposes is the FLAIR spectrum of LS4784, a typical early-type star (see Sect. 3.1).

Below we discuss the atmospheric parameters for each group of preliminary spectral-types. To simplify the discussion, stars are represented by two numbers (in square brackets) representing the field and the star:

Early-B-type candidates: For our ten candidates, eight appear to be in the high effective temperature limit of the

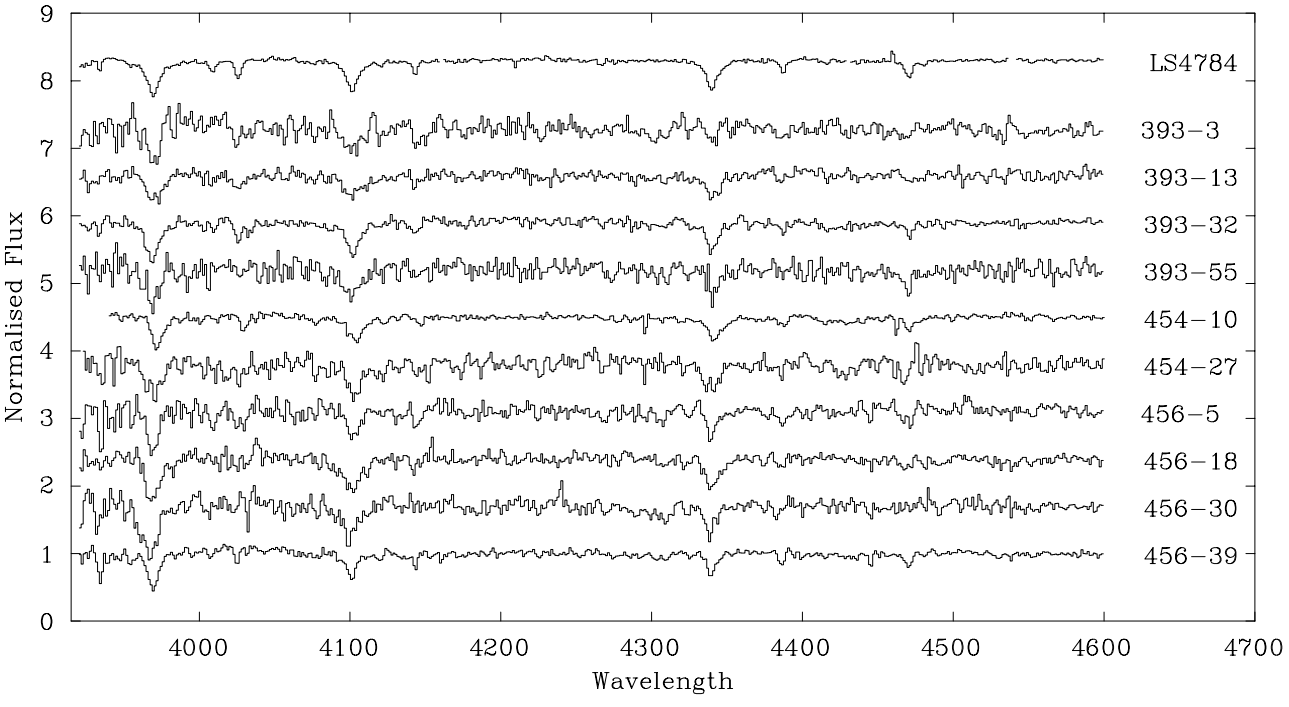

Fig. 4. Blue spectra for the early B-type candidates that we have identified. For comparison, we also show a FLAIR spectrum of LS4784 which has been previously confirmed to be a B2 IV star from high resolution data (Smartt et al. 1999)

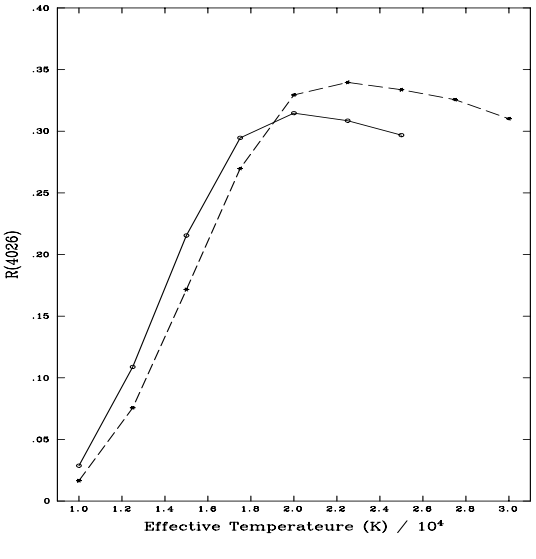

Fig. 5. The ratio, $R(4026)$, of the equivalent width of the He I line at 4026 Å to the mean equivalent width of the Hγ and Hδ lines (W_λ) is plotted as a function of effective temperature. Ratios are shown for two logarithmic gravities, viz. solid line - log $g = 3.0$; dotted line - log $g = 4.0$

line ratios and we are therefore only able to give lower limits for both the temperature and gravity. For four targets ([393,03],[393,13],[393,32] and [454,10]), these values should be secure; for the other four targets, uncertainties in the line strength implies that it is possible (but unlikely) that these stars might have lower temperatures than 20 000 K. Assuming that these stars are main (or near) main sequence stars with logarithmic gravities less than 4.2 dex (Claret 1995), then we can constrain the upper values of their effective temperatures. These would range from 24 000 K for [393,55] to 30 000 K for [393,03] and are consistent with the lack of an observed He II spectrum. For example, at an effective temperature of 30 000 K and a logarithmic gravity of 4.0 dex, our model atmosphere calculations of the He II line at 4541 Å predicts an equivalent width 0.2 Å, which increases rapidly with temperature.

Two stars have ratios that imply effective temperatures of approximately 18 000 K but in these cases the observational uncertainties are consistent with them being in the high temperature limit. However if these are main sequence targets, then their effective temperatures cannot be greater than approximately 20 000 K as this would lead to too large an estimate for the gravity. Encouragingly, for all ten targets the estimated atmospheric parameters are consistent with our original spectral classification, although our preliminary identification of [456,39] as possibly helium rich is not supported by the equivalent width estimates. In fact the helium to hydrogen line ratios for this star are all close to the high temperature limits. We further checked that none of these objects have been identified in previous catalogues and found no possible known counterparts in SIMBAD.

Mid-B-type candidates: Atmospheric parameters could be estimated for all the stars apart from [393,24]. Its spectrum was of low quality and although the helium lines appear to be present, they could not be reliably

measured. We have taken the conservative approach that their equivalent widths were less than 1 Å to estimate limits. Although the He I line strengths for the other stars are often poorly determined, they vary rapidly with the effective temperature. Hence the estimates of the atmospheric parameters should normally be reliable.

Our effective temperature estimates range from 11 000 to 16 000 K and indicate that our selection criteria have led to a homogeneous sample. However although characterised as mid-B spectral type, the adopted criteria have also included some of the later-B spectral types. This reflects the difficulty of discriminating by eye between a range of weak neutral helium line strengths. Most of the stars appear to be on (or near) the main sequence but a significant minority (eight stars) have lower gravities. These are likely to be a mixture of relatively young giants and old evolved stars (such as the post-asymptotic-giant-branch - post-AGB - objects discussed by McCausland et al. 1992). With the current data it is not possible to distinguish between these possibilities. The lack of emission in the Balmer Hα line for the targets in the Field 456 would be consistent with the former, although we note that such emission is not present in the spectra of all post-AGB stars.

Late-B/A-type candidates: For all these stars the neutral helium lines were either absent or too weak to measure. We have therefore assumed that they have equivalent widths of less than 0.5 Å. This should be appropriate for the spectra with low counts but may be too conservative for stars, such as [393,28]; however it was not felt that the data warranted assigning different equivalent width limits to each spectrum as these would, in any case, also have been wavelength dependent. The limits on the atmospheric parameters estimates are given in Table 6 and the stars appear to fall into two groups. Five targets have maximum gravity that are consistent with them being main sequence targets, whilst the other two have lower gravities. As for the previous group, these may either be relatively young stars evolving from the hydrogen main sequence or older post-AGB objects.

4. Discussion

For the three fields surveyed, we have identified 10 B-type stars with effective temperature, $T_{\rm eff} \geq 18\,000$ K and an additional 18 targets with $11\,000 \leq T_{\rm eff} \leq 18\,000$ K. Given the relatively small number in our samples, the targets seem to be uniformly distributed over the fields. There does not appear to be a strong correlation between the photographic colours and the estimated effective temperatures. For example, in our hottest sample of stars only two ([393,03] and [456,05]) have particularly blue colours with others (e.g. [393,55]) lying close to the red end cut-off of our sample. This may reflect a combination of two factors, viz. intrinsic errors in our colour determinations (that were estimated in Sect. 2.1 to be of the order of 0.2 magnitudes) and spatial variations in the reddening. However a consequence of this lack of correlation (and the blending problems discussed in Sect 2.1) is that we cannot be certain that our sample of early-type objects is complete.

We have estimated the distances to the stars as follows. For the early-B-type group, we have assumed a typical spectral type of B2V and a corresponding absolute V magnitude of -2.4 (Schmidt-Kaler 1982). The largest uncertainty is in the interstellar extinction and here we have just adopted the value of $E(B-V) \simeq 0.3$ for LS4825 – a star, which is believed to be beyond the galactic centre (Ryans et al. 1997) and has $b = -6.6°$. Then most of our early-type targets lie in a magnitude range of $12.5 \lesssim V \lesssim 16.0$, which would map onto a distance scale of 6 to 30 kpc. Similarly for the mid-B-type subgroup, adopting an absolute V magnitude of -1.0 and an apparent magnitude range of $10.5 \lesssim V \lesssim 15.0$ would lead to distances from 1.3 to 10 kpc. We should emphasise that given the unknown (and possibly highly variable) extinction towards these targets, we consider these distance estimates to be illustrative. However, given that most of the early B-type candidates have galactic coordinates which indicate that they may sit slightly out of the plane (Table 7), one would expect that they would have similar reddenings (and hence distances) to the distant objects discussed in Smartt et al. (1997, 1999). The latter have $2° \leq |b| \leq 10°$, similar to the values shown in Table 7, and have reddenings in the range $0.3 < E(B-V) < 0.5$. If these values are equally applicable to our newly identified stars, then their magnitudes and approximate atmospheric parameters would be compatible with them being near-galactic centre objects.

As discussed above, at least some of our early-type stars may be subluminous and evolved. Indeed it is interesting that the apparent magnitude range for the early-B-type stars is approximately one magnitude fainter ($12.5 \lesssim V \lesssim 16.0$) than that for their mid-B-type counterparts ($10.5 \lesssim V \lesssim 15.0$). This is despite the former being intrinsically brighter by one to two magnitudes, if they are young hydrogen burning objects. Hence at least for the early-B-type stars, our sample may be contaminated by post blue-horizontal-branch (post-BHB) and post-AGB stars (see, for example, Hambly et al. 1997, and references therein). Alternatively it may just reflect the relatively small sample sizes or a different spatial distribution.

Our early-B-type objects have gravities of $3.2-4.0$ dex (adopting their lower effective temperature limit of 20 000 K for all stars apart from [456,18] and [456,30]); alternatively if a typical effective temperature of 25 000 K was assumed their gravity range would be approximately $3.6 - 4.2$ dex. The evolutionary tracks of Schönberner (1993 and references therein) implies that post-AGB stars have gravities in the ranges $2.4-3.4$ and $2.8-3.8$ dex for effective temperatures of 20 000 and 25 000 K respectively. By contrast a post-BHB star with a mass of 0.5 $M_{\odot}$ has a gravity of ≥ 3.7 dex for an effective temperature $\leq$ 25 000 K (Castellani et al. 1994). Hence although some of our candidates could be post-AGB stars they

Table 7. Galactic Coordinates of the early B-type candidates. Most of these objects lie slightly out of the plane, at similar latitudes to the objects discussed in Smartt et al. (1999), and Ryans et al. (1997). Hence they should have similar low-moderate reddenings and are potentially distant, massive stars

Field	Star	l°	b°
393	3	354.81	−4.20
393	13	355.39	−1.31
393	32	354.91	−3.90
393	55	351.76	−1.91
454	10	356.85	+5.27
454	27	354.39	+4.38
456	5	1.07	−6.44
456	18	1.34	−5.48
456	30	1.25	−6.30
456	39	2.74	−3.44

are more likely to be post-BHB stars. In any case, if they are evolved then independent of their exact evolutionary status, they would have a mass of approximately $0.5 - 0.6\ M_\odot$.

Adopting a typical mass of $10 - 12\ M_\odot$ for a main sequence early-B-type star (Schaller et al. 1992), leads to a mass ratio between the two evolutionary scenarios of approximately 20. Hence if all our early-B-type sample were evolved, their range of distances estimated above would be reduced to approximately 1−6 kpc. Although this possibility cannot be excluded, our identification of normal early-B-type stars towards the galactic centre (Smartt et al. 1997, 1999) makes it unlikely. Hence we conclude that although some of our early-type candidates are probably evolved, the sample should also contain young hydrogen burning stars.

Acknowledgements. We wish to thank the staff of the Anglo-Australian Observatory and UKSTU at the Royal Observatory Edinburgh for obtaining additional Schmidt plates and for assistance with the low dispersion spectroscopy. We are grateful to Harvey MacGillivray and Eve Thomson for measuring the plates on SuperCOSMOS. Part of the data reduction was undertaken on the PPARC funded Starlink node at Queen's University. PPARC financial support including that for a visiting fellowship programme at QUB is gratefully acknowledged.

References

Beard S.T., MacGillivray H.T., Thanisch P.F., 1990, MNRAS 247, 311
Blanco V.M., Blanco B.M., 1984, PASP 96, 603
Conlon E.S., Dufton P.L., Keenan F.P., McCausland R.J.H., 1993, ApJ 408, 593
Castellani M., Castellani V., Pulone L., Tornambe A., 1994, A&A 290, 897
Claret A., 1995, A&AS 109, 441
Drinkwater M., Holman B., 1996, Flair Data Reduction with IRAF. AAO Internal publications
Dufton P.L., 1998, Proceedings of the BMW-II conference, ASP Conf. Ser. 169
Gies D.R., Lambert D.L., 1992, ApJ 387, 673
Hambly N.C., Miller L., MacGillivray H.T., Herd J.T., Cormack W.A., 1998, MNRAS 298, 897
Hambly N.C., Rolleston W.R.J., Keenan F.P., Dufton P.L., Saffer R.A., 1997, ApJS 111, 419
Hibbins R.E., Dufton P.L., Smartt S.J., Rolleston W.R.J., 1998, A&A 332, 681
Howarth I.D., Murray J., Mills D., 1993, Starlink User Note 50.14
Kilian J., 1992, A&A 262, 171
Kudritzki R.P., 1998, Proceedings of the 7th Canary Island Winter School (in press)
Kurucz R.L., 1991, Precision Photometry: Astrophysics of the Galaxy, Philip, Upgren and Janes (eds.). L Davis Press, Schenectady
McCarthy J.K., Lennon D.J., Venn K.A., Kudritzki R.P., et al., 1995, ApJL 455, 135
McCausland R.J.H., Conlon E.S., Dufton P.L., Keenan F.P., 1992, ApJ 394, 650
Monteverde M.I., Herrero A., Lennon D.J., Kudritzki R.P., 1997, ApJL 474, 107
Parker Q.A., Watson F.G., 1994, IAU Symposium No. 161, 85
Perek L., Kohoutek L., 1967, Acad. Publ. House of the Czech. Acad. Sci. 1
Reed B.C., 1993, ApJS 87, 367
Reed B.C., Beatty A.E., 1995, ApJS 97, 189
Rolleston W.R.J., Dufton P.L., Fitzsimmons A., Howarth I.D., Irwin M.J., 1993, A&A 277, 10
Rolleston W.R.J., Brown P.J.F., Dufton P.L., Howarth I.D., 1996, A&A 315, 95
Ryans R.S.I., Dufton, P.L. Keenan F.P., Smartt S.J., et al., 1997, ApJ 490, 267
Schmidt-Kaler T., 1982, Landolt-Berstein VI 2b, 1
Schaller G., Schaerer D., Meynet G., Maeder A., 1992, A&AS 96, 269
Schönberner D., 1993, IAU Symp. 155, 415
Smartt S.J., Rolleston W.R.J., 1997, ApJL 481, 47
Smartt S.J., Dufton P.L., Rolleston W.R.J., 1996a, A&AS 116, 483
Smartt S.J., Dufton P.L., Rolleston W.R.J., 1996b, A&A 310, 123
Smartt S.J., Dufton P.L., Lennon D.J., 1997, A&A 326, 763
Smartt S.J., Venn K.A, Lennon D.J., Dufton P.L., Rolleston W.R.J., 1999, A&A (submitted)
Stobie R.S., Kilkenny D., O'Donoghue D., et al., 1997, MNRAS 287, 848
Szmanski M., Udalski A., Kubiak M., et al., 1996, Acta Astron. 46, 1
Tritton S.B., 1983, United Kingdom Schmidt Telescope Handbook, Royal Observatory Edinburgh
Urban S.E., Corbin T.E., Wycoff G.L., 1998, AJ 115, 2161
Valdes F., 1992, Guide to Multifiber Reduction Task DOFIBERS, NOAO
Venn K.A., Smartt S.J., Lennon D.J., Dufton P.L., 1998, A&A 334, 987
Walker A.R., Mack P., 1986, MNRAS 220, 69